

# Electric field-induced exciton localization in quantum wells

Karsten Sperlich<sup>1</sup>, Patrick Ludwig<sup>1,2,\*</sup>, Alexei Filinov<sup>2</sup>, Michael Bonitz<sup>2</sup>, Heinrich Stolz<sup>1</sup>, Detlef Hommel<sup>3</sup> and Arne Gust<sup>3</sup>

<sup>1</sup> Institut für Physik, Universität Rostock, D-18051 Rostock, Germany

<sup>2</sup> Institut für Theoretische Physik und Astrophysik, Christian-Albrechts-Universität zu Kiel, D-24098 Kiel, Germany

<sup>3</sup> Institut für Festkörperphysik, Universität Bremen, D-28334 Bremen, Germany

Received XXXX, revised XXXX, accepted XXXX

Published online XXXX

PACS 71.10.-w; 71.35.-y; 78.20.Jq; 78.67.De; 73.21.-b; 03.75.Lm

\* Corresponding author: e-mail ludwig@theo-physik.uni-kiel.de, Phone +49-(0)431-8804732, Fax +49-(0)431-8804094

We report on first spectrally and spatially high resolved measurements of a recently suggested electrostatic confinement [Ludwig *et al.*, *phys. stat. sol. (b)* **243**, No. 10, 2363 (2006)] for excitons in a single quantum well.

For this strongly correlated many-particle system we present finite-temperature quantum Monte-Carlo results and discuss the specific trap parameters at which a phase transition to a mesoscopic Wigner crystal phase of spatially indirect excitons is expected to be accessible.

Copyright line will be provided by the publisher

**1 Introduction.** Excitonic systems in external trapping potentials are of paramount interest for several recent research issues since they allow to realize and control strong correlation and quantum effects. Examples include the theoretically predicted Bose Einstein Condensation, e.g. [1]-[5], or the Wigner crystallization of indirect excitons in semiconductor heterostructures [6]-[9]. Different types of traps for excitons have been suggested and implemented such as natural traps [10], pressure [11], laser [12], magnetic field [13], and electrostatic field induced traps [14-16]. However, these traps typically possess only *one free parameter* which defines both, the exciton and trap properties.

Here we will focus on a recently proposed electrostatic setup [17], which consists of an adjustable conducting tip above the single quantum well (QW) sample (see inset Fig. 1). The considered quantum Stark confinement provides essentially *two degrees of freedom*: (i) the height  $z_{tip}$  of the tip relative to the sample surface, which allows to vary the lateral confinement strength of the basically harmonic trap geometry, and (ii) the tip voltage  $U$  allowing for control of the electron-hole separation, i.e. a voltage-controlled transition from the (spatially) direct to the indirect exciton regime [18]. The field-induced indirect excitons possess a (cross-well) permanent electric dipole mo-

ment, which gives rise to a strong repulsive exciton-exciton interaction.

**2 Experimental setup.** Due to the small trap size on the micrometer scale an advanced optical setup is required for spatially resolved spectroscopy. Also, the sample must be cooled down to ensure that the exciton levels are not destroyed by thermal effects. The complexity of the setup is particularly increased by the fact that the optimal distance  $z_{tip}$  is about only several micrometers, which requires the tip and its positioner to be located inside the cryostat. It turned out to be useful to have a static optical setup and move the cryostat for selecting a position of the sample and to adjust the focus. A microscope objective with 11 mm working distance was used together with a set of lenses to realize an optical setup according to Köhler to minimize optical losses. A cylindrical lens corrects the astigmatism of the used Raman spectrometer. The field of view is about 250  $\mu\text{m}$  which implies some further effort to locate the projection of the tip on the sample surface of 4  $\text{mm}^2$  size. For optical inspection of the tip and the sample surface, as well as for reflection measurements we used a high power single chip LED (Seoul P4 cold white) which has an intensity peak in the blue region. Luminescence measurements were done with a fs-pulsed laser above the band edge

Copyright line will be provided by the publisher

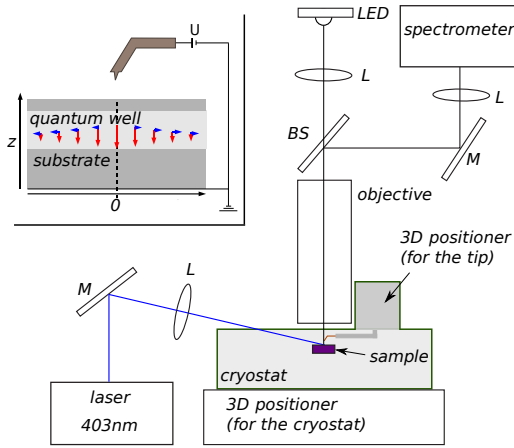


**Figure 1** Schematic setup (L: lens, M: mirror, BS: beam splitter). The inset shows the exciton trap with two degrees of freedom: tip to sample distance  $z_{tip}$  and voltage  $U$ . The harmonic in-plane confinement for the neutral excitonic system is generated by the inhomogeneous electrostatic  $z$ -field of a fine tip electrode due to the quantum-confined Stark effect. The arrows in the QW plane indicate the lateral (blue) and cross-well (red) field components.

( $E_{gap,dir} = 2.822\text{eV}$ ). Excitation power was about  $15\text{mW}$  with  $300\mu\text{m}$  spot size.

Due to the fact that we analyze the luminescence light and the reflected light perpendicular to the sample surface, the tip reduces ('shadows') the analyzed light. Thus, in the present setup the minimum  $z_{tip}$  is limited to about  $50\mu\text{m}$ . To achieve the required field strengths for the electron-hole separation on the order of  $10^6\text{V/m}$  for a finite range of  $z_{tip}$ -distances the applied voltage needs to be in the range of several kV. The tip used in the present measurements was etched from a  $100\mu\text{m}$  tungsten wire and has a tip diameter of  $13\mu\text{m}$ .

**3 Luminescence measurements.** Here we present first luminescence measurements of a  $28\text{nm}$  wide ZnSe QW at  $40\text{K}$ ,  $z_{tip} = 50\mu\text{m}$  and  $U = 3\text{kV}$ . We expect the field strength to be about  $10^6\text{V/m}$  in the center of the trap (in the QW plane below the tip). The low intensity makes it necessary to integrate over 20 lines of the CCD chip to achieve a reasonable signal to noise ratio.

In Fig. 2 we compare two measurements, one with trap potential (red curve) and one without (black curve). The luminescence shows in both cases a number of lines, which we attribute to heavy hole (hh) and light hole (lh) polariton resonances as indicated in the figure. This is quite similar to the polariton effects in transmission [20] or reflection [21] spectroscopy of the same sample. Since the emission peak mainly results from the increased transmission of the sample at the resonance, a more closer inspection shows that the absolute energy positions are shifted about  $1.5\text{meV}$  due to the higher measurement temperature. The splitting between hh and lh is slightly larger in Ref. [20], probably

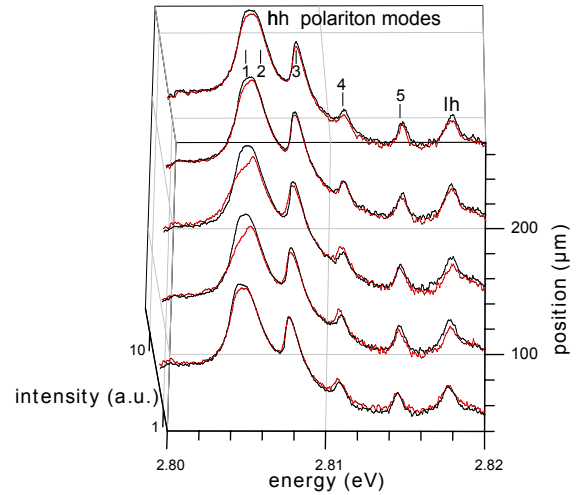


**Figure 2** Spatially resolved luminescence of ZnSe with (red) and without (black) trap potential (hh: heavy hole, lh: light hole). The trap center is located at  $r_0 = 125\mu\text{m}$ . ( $T = 40\text{K}$ )

due to removing the substrate which results in a different stress tensor and hence influences the hh-lh splitting. Similar to Ref. [20], the hh peak actually consists of to the first polariton resonance near  $k = 0$  at the low energy side and the second polariton resonance at the high energy side. Both from our calculations and from the simple excitonic Stark shift given in [22] we expect the hh state to shift to lower energies amounting to about  $-1.5\text{meV}$  at the maximum field strength. In our experiments we instead observe a relative intensity change of the hh peak occurring at the low energy side. This corresponds to a reduced intensity of the first polariton mode compared to the second polariton mode. Field ionization of the excitons may be a reason. According to [17] this is expected to occur above  $2 \cdot 10^6\text{V/m}$ . With respect to the present sample (exciton binding energy is  $17\text{meV}$ ), we expect field ionization at even lower field strength. The missing energy shift can be explained by the different band offsets (conduction band:  $2.1\text{meV}$ ; valence band:  $20.6\text{meV}$  [20]) in the used sample. The smaller conduction band offset reduces the localization of the electron in the quantum well compared to the hole. That results in a much smaller energy change by the quantum confined Stark effect because the electron wave function can adjust itself to the hole. Therefore no spatially indirect excitons are created. Using a sample with equal band offsets solves that problem whereas a slightly thinner quantum well will help to overcome the field ionization and even clear the way for higher field strength. That can be easily achieved by integrating a back electrode in the sample. Thereby also the in plane field can be reduced, that currently destabilizes (or even destroys) the excitons [17, 19].

**4 Theoretical perspectives.** At low temperatures (well below the exciton binding energy) and small electron-hole separations  $d$  the electrons and holes form stable spa-

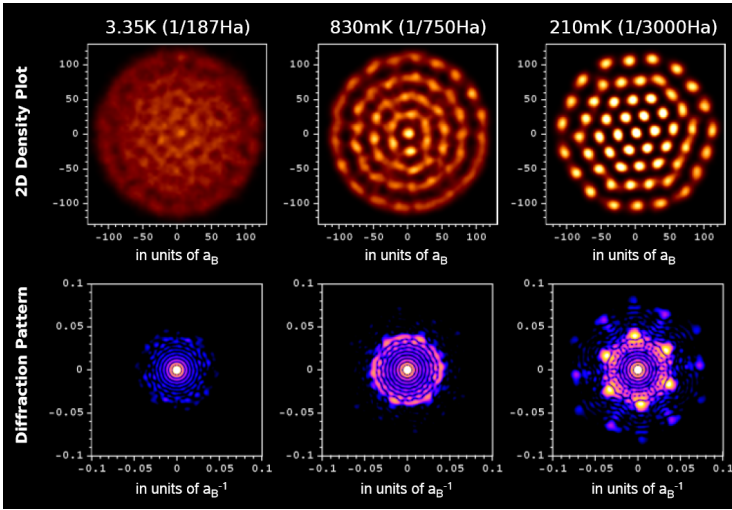


**Figure 3** PIMC results for 56 trapped indirect excitons obeying Bose statistics. Effective spatial electron-hole  $z$ -separation  $d = 20\text{nm}$  ( $6.6a_B$ ).

Top row: Exciton density plots for three temperatures: 3.35K, 830mK and 210mK (from left to right). Due to strong inter-exciton correlations highly ordered quantum states are observed; reducing temperature initiates a two-stage crystallization process: (1) radial ordering of the excitons on shells, (2) formation of a bosonic Wigner nano-crystal with a hexagonal lattice structure. Partial exciton delocalization is a result of quantum fluctuations and Bose statistics (“cold” melting). The plots are averaged over  $10^5$  PIMC steps (plus  $10^5$  steps for equilibration), number of high temperature factors  $M = 362$  (PIMC, for details see [24]).

Bottom row: Corresponding diffraction patterns as an indicator of a phase transition (logarithmically scaled).

tially indirect excitons [19]. Previous results, where the Fermi statistics of the exciton constituents was fully taken into account [5], have shown that in the moderate density regime the indirect excitons maybe be treated as composite Bose particles. In particular at a considered in-plane density regime of  $1.5 \cdot 10^{10}/\text{cm}^2$ , the electron-hole binding energy of an individual exciton is much stronger than the repulsive exciton-exciton interaction ( $U_{eh} \gg U_{xx}$ ). Introduction of relative and center of mass (COM) coordinates of the composite excitons allows us for a separation of the  $z$ -problem by averaging over the QW thickness by solving the single exciton problem for the QW confinement (presented as a square well) in the presence of the electric field [19]. Hence, the problem reduces to an effective 2D-Hamiltonian

$$\hat{H}_x = \sum_{i=1}^{N_x} \left[ \frac{-\hbar^2}{2m_x^*} \nabla_{\mathbf{R}_i}^2 + \frac{m_x^*}{2} \omega_0^2 \mathbf{R}_i^2 + \sum_{i < j}^{N_x} \frac{\mu(\mathbf{R}_i)\mu(\mathbf{R}_j)}{\varepsilon |\mathbf{R}_i - \mathbf{R}_j|^3} \right]$$

for  $N_x$  composite bosonic excitons with the effective dipole moment  $\mu(\mathbf{R}) = ed(\mathbf{R})$  in a harmonic lateral (quantum Stark) confinement potential and a repulsive dipole interaction potential as discussed in [17, 19]. The COM coordinate  $\mathbf{R}_i$  describes the in-plane position of the  $i$ -th exciton in the external potential. Further,  $e$  denotes the elementary charge,  $\varepsilon$  the static permittivity,  $m_x^*$  the effective exciton mass and  $\omega_0$  the in-plane trap frequency. The problem of  $N_x$  indirect excitons is solved by *Path Integral Monte Carlo* (PIMC) simulations, which allow for a first principle treatment of the many-particle Coulomb correlation and bosonic exchange effects. Details on the applied PIMC technique are given in [24].

In the following we will consider the representative example of a mesoscopic system consisting of 56 spin-polarized indirect excitons with an effective electron-hole pair separation of  $d = 20\text{nm}$ . This carrier separation can be produced by an electric field of strength  $E_z = 20\text{kV/cm}$  in a single ZnSe-based QW of 30nm width [17]. Quantitative

predictions on the excitonic states of the considered exciton cluster for three specific temperatures are presented in Fig. 3. Our simulations point out that the particles become highly correlated and can even freeze into spatially periodic structures when the temperature is decreased below a critical value of  $T_{cr} \lesssim 1.2\text{K}$ . Interestingly, a two-stage Wigner crystallization process is observed:

1. At the temperature 3.35 K, i.e., slightly above the finite melting interval [27, 28], the indirect excitons are in a Bose fluid state and delocalized within the trap due to thermal fluctuations as well as quantum fluctuations and bosonic exchange.
2. When the temperature is decreased to 830 mK the indirect excitons become strongly correlated and enter a partially ordered state. The particles arrange themselves on four distinct rings (a single exciton is located in the trap center). Note that the concentric shell structure reflects the radial symmetry of the external confinement.
3. Further lowering of temperature to 210 mK leads to a freeze-out of the thermal fluctuations, whereby the (zero-point) quantum fluctuations prevail. The PIMC simulations show that the repulsive inter-exciton interaction exceeds the quantum fluctuations and gives rise to an intrashell localization of the quasi-particles. A highly ordered quantum state with a hexagonal 2D Wigner lattice is observed in the center region of the trap (where the geometrical constraints of the external confinement are reduced).

The two-stage transition process is a well-known phenomenon in 2D confined few-particle systems, e.g. mesoscopic electron systems [25, 26]. This is due to the fact that the confinement induced radial energy barriers are considerably higher than the intrashell energy barriers separating the repelling particles. Because of the short range of the dipole potential, the mesoscopic quantum crystal of indirect excitons appears at higher densities than the electron

(Coulomb) Wigner crystal, i.e. the crystal is stabilized. Previous numerical work predicts a transition from the Fermi liquid state to the electron Wigner crystal phase for around  $r_s^e \approx 35$  (see [25,26] and references therein), whereas in the present simulations the exciton Bose-nano-crystal is already found at  $r_s^x \approx 25$ .<sup>1</sup>

A deeper insight into the structural features of the different exciton phases can be obtained from the diffraction picture, with the motivation that emergence of a discrete diffraction diagram indicates a structural phase transition (in the mesoscopic system) [29]. The diffraction intensity is obtained from the spatial 2D Fourier transform of the (time averaged) exciton density distribution  $\rho(\mathbf{r})$

$$I(\mathbf{h}) = \left| \int_{-\infty}^{+\infty} \rho(\mathbf{x}) e^{i2\pi\mathbf{h}\mathbf{x}} d^2x \right|^2,$$

and is parametrized by the in-plane (transfer) vector  $\mathbf{h}$ . Let us now study the diffraction diagram of the exciton cloud for the characteristic temperatures displayed in Fig. 3. The diagram for 3.35 K reveals (beside the divergent central spot due to long-wavelength fluctuations) five weak circular symmetric side maxima. These are a first signature of the growing *inter-exciton correlations* and the onset of a radial density modulation. Lowering the temperature to 830 mK leads to pronounced circular main maxima in the diffraction intensity at  $h = 0.04/a_B$ , which corresponds to an almost equidistant radial density modulation (resp. intershell spacing) of  $25 a_B$ . Unlike the main peaks, which are also found in larger clusters, the number of ( $n-2=7$ ) subsidiary maxima and ( $n-1=8$ ) subsidiary minima are affected by the finite size of the cluster, i.e., the  $n=9$  density peaks in the center cross section of the shell structure. However, the most interesting and richest diffraction pattern is found at 210 mK, where the central region of the mesoscopic exciton crystal presents a hexagonal lattice symmetry in real space with spacing of  $25 a_B$ . The 2D hexagonal lattice (which is known for lowest energy in the unconfined case) gives rise to six distinct intensity peaks in the diffraction image with the Brillouin zone appearing as a hexagon. The existence of a discrete diffraction picture indicates a phase transition of the mesoscopic exciton gas into a crystalline state (i.e. a 2D crystal without conventional long-range order).

The finding of the exciton Wigner crystal phase raises the question about the coherence of this quantum state. In particular the finite size of the trapped system may allow for a fully phase coherent state of indirect excitons even in 2D, where the coherence length cannot be infinite. In this context it should be mentioned, that even in the Wigner

crystal phase single density peaks do not necessarily correspond to single particles (excitons). Even in the crystal state single-particle orbitals can extend over the entire cluster as was shown by orbital resolved calculations [23]. The question about the quantum coherence properties of the exciton fluid and Wigner crystal state (including superfluidity) remains a fascinating topic for further theoretical and experimental work.

**5 Conclusion.** The presented setup should allow for experimental observation of field-induced localization of an exciton cloud within a mesoscopic confinement. Furthermore, at temperatures slightly below 1 K the strong repulsion between the indirect excitons is expected to establish a crystal-like state of excitonic matter with strong bosonic many-particle features. The next series of measurements is projected with a sample with roughly equal band offsets and 20 nm quantum well and a back electrode close to the QW. In combination with the recently installed dilution cryostat with a base temperature of about 20 mK the stage is set for exciting measurements on mesoscopic structures in the millikelvin temperature range and should allow for the investigation of prominent many-particle effects including the Wigner crystal phase of spatially indirect excitons.

## References

- [1] L.V. Keldysh and A.N. Kozlov, Zh. Eksp. Teor. Fiz. **54**, 978 (1968); Sov. Phys. JETP **27**, 521 (1968)
- [2] A. Griffin, D.W. Snoke, and S. Stringari (eds.), *Bose-Einstein Condensation*, Cambridge, New York (1995)
- [3] S. De Palo *et al.*, Phys. Rev. Lett. **88**, 206401 (2002)
- [4] J. Shumway, and D.M. Ceperley, Solid State Comm. **134**, 19 (2005)
- [5] A. Filinov *et al.*, phys. stat. sol. (c) **3**, No. 7, 2457 (2006)
- [6] A. Filinov *et al.*, phys. stat. sol. (c) **0**, No. 5, 1518 (2003)
- [7] Yu.E. Lozovik *et al.*, JETP Letters **79**, No. 10, 473 (2004)
- [8] C. Mora *et al.*, Phys. Rev. B **76**, 064511 (2007)
- [9] G.E. Astrakharchik *et al.*, Phys. Rev. Lett. **98**, 060405 (2007)
- [10] L.V. Butov *et al.*, Nature **417**, 47 (2002)
- [11] V. Negoita *et al.*, Phys. Rev. B **60**, 2661 (1999)
- [12] A.T. Hammack *et al.*, Phys. Rev. Lett. **96**, 227402 (2006)
- [13] P.C.M. Christianen *et al.*, Physica B **249**, 624 (1998),
- [14] R. Rapaport *et al.*, Phys. Rev. B **72**, 075428 (2005)
- [15] A.T. Hammack *et al.*, J. Appl. Phys. **99**, 066104 (2006)
- [16] V.B. Timofeev *et al.*, J. Phys.: Cond. Matt. **19**, 295209 (2007)
- [17] P. Ludwig *et al.*, phys. stat. sol. (b) **243**, No. 10, 2363 (2006)
- [18] V.V. Solov'ev *et al.*, JETP Letters **83**, 553 (2006)
- [19] A. Filinov *et al.*, J. Phys: Conf. Series **35**, 197 (2006)
- [20] S. Schumacher *et al.*, Phys. Rev. B **70**, 235340 (2004)
- [21] M. Seemann *et al.*, phys. stat. sol. (c) **3**, 1610-1634 (2006)
- [22] M. Fox, *Optical Properties of Solids*, Oxford University Press, 131 (2001)
- [23] P. Ludwig *et al.*, New J. Phys. **10**, 083031 (2008)
- [24] M. Bonitz and D. Semkat (eds.), *Introduction to Computational Methods in Many Body Physics*, Rinton Press, Princeton (2006)

<sup>1</sup> We define  $r_s^e$  ( $r_s^x$ ) as the first peak of the electron (exciton) pair distribution function in units of the effective electron Bohr radius  $a_B = \hbar^2\epsilon/m_e^*e^2 = 3.07$  nm. The used ZnSe parameters are  $\epsilon = 8.7$ , electron mass  $m_e^* = 0.15m_0$ , hh mass  $m_{hh}^{*(xy,z)} = (0.37, 0.86)m_0$  (with free electron mass  $m_0$ ).

- [25] A. Filinov *et al.*, Phys. Rev. Lett. **86**, 3851 (2001)
- [26] A. Ghosal *et al.*, Nature Physics **2**, 336 (2006)
- [27] A. Proykova and R.S. Berry, J. Phys. B: At. Mol. Opt. Phys. **39**, R 167 (2006)
- [28] J. Böning *et al.*, Phys. Rev. Lett. **100**, 113401 (2008)
- [29] Foundations of Crystallography, *IUCr: Report of the Executive Committee for 1991*, Acta Crystallogr. **A48**, 922 (1992)